*ICANS-XI International Collaboration on Advanced Neutron Sources*
*KEK, Tsukuba, October 22-26, 1990*

# NEUTRON SCATTERING ON ROTAX

H. Tietze [a,b], W. Schmidt [a], R. Geick [a], U. Steigenberger [c], H. Samulowitz [d]

a) Physikalisches Institut der Uni Würzburg, Am Hubland, 8700 Würzburg, F.R.G.
b) IFF der KFA Jülich, Pf 1913, 5170 Jülich, F.R.G.
c) Neutron Division Rutherford Appleton Lab., Chilton, U.K.
d) HEWATT GmbH, Am Hahnenkreuz 46, 5190 Stolberg-Dorff, F.R.G.

## Successful coherent inelastic and elastic neutron scattering on ROTAX !

ROTAX is an inverted time-of-flight spectrometer for neutron inelastic scattering of single crystals at ISIS. Its particular technical highlight is the performance and utilisation of its nonuniformly rotating crystal analyser, which is time synchronised with the neutron source. However, the parameters determining a particular mode of operation or time-of-flight scan through $(Q,\omega)$-space are, in general, kept free with respect to the individual demand of the experimentalist. The user of the instrument may thus program his personal particular scan, providing much more flexibility and versality for an inelastic coherent scattering experiment at a pulsed spallation source taking advantage of the time structure and utilising not only the average neutron flux.

At realistic conditions of the geometry and neutron optics, prototypes of the ROTAX spectrometer have been critically andfirmly tested on the S9 test beam facility at ISIS, in order to confirm and prove the ability and stability of the technical design of the ROTAX-analyser drive.

Throughout this paper we shall concentrate on the results of these test experiments with the ROTAX analyser drive, particularly on elastic and inelastic neutron scattering at an aluminium single crystal, where acoustic phonons have been measured directly in longitudinal and transverse polarisation. Precursory alignment of the test apparatus will be explained and the intensity performance of the ROTAX "lighthouse mode" will be discussed in comparison to the PRISMA-mode of a non-spinning idle analyser as used in conventional TOF-X spectrometers.

## I. Introduction

ROTAX stands for rotating analyser crystal spectrometer which is a highly flexible time-of-flight neutron spectrometer of inverted geometry with one single crystal analyser. By means of a user defined, programmable non-uniform rotation of the analyser crystal several types of scans in $(Q,\omega)$-space can be performed [1], e.g. const.-energy or const.-$\vec{Q}/Q$ scans. The scope of the instrument will be neutron inelastic scattering investigations on collective excitations of single crystalline samples. In some sense ROTAX will compete with triple axis spectrometers at reactor thermal beam lines and of course with conventional TOF-crystal analyser spectrometers installed at pulsed spallation sources, e.g. with the Constant-Q spectrometer at LANCE [2] and with the high-symmetry spectrometers MAX at KENS [3] and PRISMA at ISIS [4,5]. As discussed earlier [6] the major advantage of ROTAX in comparison to the above mentioned spectrometers is to provide the user with an instrument with a much higher degree of flexibility in the choice of scans. Thus, ROTAX will quite considerably improve the work in the field of single crystal collective excitations at pulsed sources. Set-up and optimisation of ROTAX scans with respect to the analyser-motor performance have been discussed earlier [7]. A detailed description of technical ROTAX concept, the electronic control of the regulation loop, the feed-back, logic and hardware configuration is also given in [7].

The basic idea of the instrument is to analyse by Bragg reflection all the neutron energies being scattered during one ISIS pulse from a sample placed in a white pulsed beam. During the neutron flight time between the moderator and the sample, the neutron pulses will disperse in energy and time (cf. fig.1).

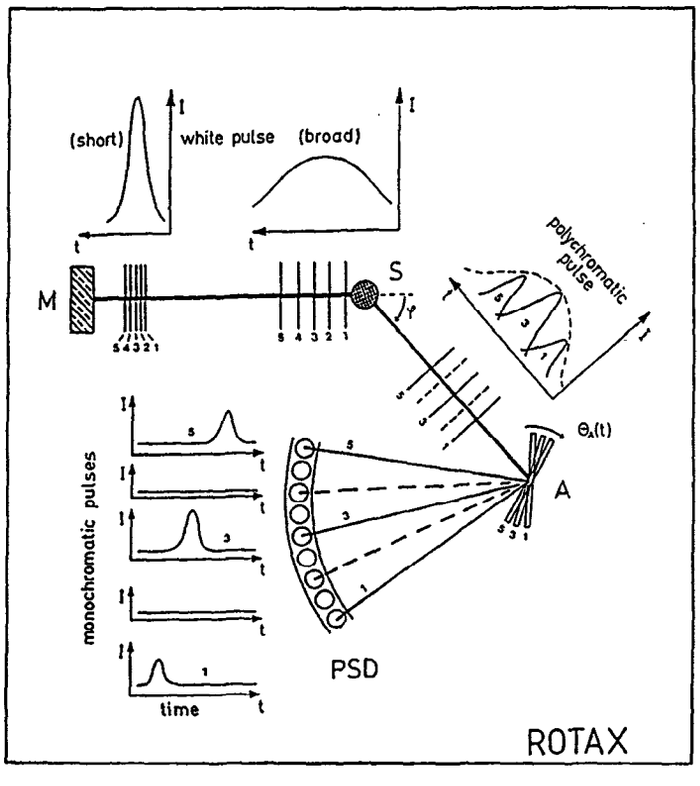


Fig. 1. Schematic diagram of ROTAX and neutron the pulse propagation.
M: moderator, S: sample, A: analyser, PSD: detector.

According to the scattering function of the sample, the neutrons will then be scattered within a certain solid scattering angle $\phi$ into polychromatic sequences of neutron packages, which will reach the analyser crystal consecutively after a well defined time-of-flight. If the analyser crystal is then positioned at the appropriate time to a Bragg angle $\Theta_A(t)$ corresponding to the scattered neutron energy, it will scatter this particular neutron package into a wide angle position sensitive detector. The scattering equations involved have been determined earlier [1]; the scattering angles $\phi$ and $\Theta_A(t)$ and the total time-of-flight $t_0$ determine the energy and momentum transfer of the neutrons unambigously. In order to detect several (ideally all) of the scattered neutron energies, it is essential to turn the analyser crystal in an accelerated, non-uniform spinning mode which must be synchronised with the time structure of the neutron pulses. There is not one general function of analyser motion, but it rather varies from one scan through $(Q,\omega)$-space to another depending on the initial scan parameters as being defined by the experimentalist.

## II. Experimental set-up

The ISIS test beam facility on the S9 beam line viewing the solid methane moderator has been used to perform first neutron scattering experiments with a provisional prototype of the ROTAX spectrometer. The purpose of these test experiments was to basically demonstrate the capability and flexibility of the ROTAX principle. It was further to firmly test the prototype and our technical concept of the heart of ROTAX, the control of its synchronised analyser motor. Minimum effort was put on all the other spectrometer components of the test assembly, such as beam collimation, shielding, goniometer drive and automatisation, data aquisition and detector electronics, in order to keep them as simple and as cheap as possible.

An aluminium single crystal has been used as a sample for the tests and was placed with its (001) scattering plane directly into the white pulsed neutron beam at $L_i$ = 12.08 m incident flight path. A cylindrically shaped Germanium single crystal of 1.2 cm diameter and 5 cm height has been used as Bragg-analyser of the scattered neutron energies. It was mounted on the ROTAX analyser motor shaft, well balanced and well oriented with its <110> crystallographic axis parallel to the rotational motor axis. Its nutation amplitude has been measured to be less than 20 $\mu$m. 10 $^3$He gas tube counters, grouped in two arrays of 5 counters each, have been used as neutron detectors combined with standard RAL data acquisition electronics. The two detectors arrays and the ROTAX motor equipped with the Ge-analyser was then mounted on a double pivoting arm centered around the sample position. The reason for grouping the detectors within two arrays was to achieve sufficient angular resolution within each array in order to demonstrate the essential capability of ROTAX: i.e. to scan at least two time channels (or neutron energies) quasi-simultaneously within one frame of the neutron pulses. Fig. 2 illustrates schematically the geometric set-up, whereas the essential geometric parameters are compiled in tab. 1. As part of detector tests, one unit of the high resolution $^6$Li-glas szintillator detector bank JULIOS [8] has been used to specify details for the final detector decision for ROTAX. The JULIOS bank and its total data aquisition electronics was a loan from the powder diffractometer SV7 at the DIDO reactor at KFA Jülich, and it was especially equipped with a suitable time analysis system of at least 12 $\mu$sec time resolution in an adjustable 8 bit wide time window.

Tab. 1.: Test beam parameters as used for ROTAX test assembly:

| | | | |
|---|---|---|---|
| sample | Al single crystal | analyser plane: | |
| | | Ge-(400) | $d_A$=1.414 Å |
| sample shape | cylindrical 3.7 cm ∅, 4.8 cm height | Ge-(220) | $d_A$=1.999 Å |
| | | distances: | |
| sample orientation | <100> x <010> in scattering plane | moderator to sample | $L_i$=12.08 m |
| | | sample to analyser | $L_a$=0.595 m |
| | | sample to detector (He) | $L_f$=0.585 m |
| analyser | Ge single crystal | sample to detector (Julios) | $L_f$=0.368 m |
| analyser shape | cylindrical 1.2 cm ∅, 5 cm height | beam size at sample | 3.5 x 3.5 $cm^2$ |
| | | primary collimaion | natural in-pile |
| analyser orientation | <100> x <011> in scattering plane | secondary collimation | none |
| | | range of: | |
| analyser mosaicity | $\eta \approx 1°$ | scattering angle $\phi$: | 0° - 100° |
| | | analyser angle $\Theta_A$: | -20° - 110° |

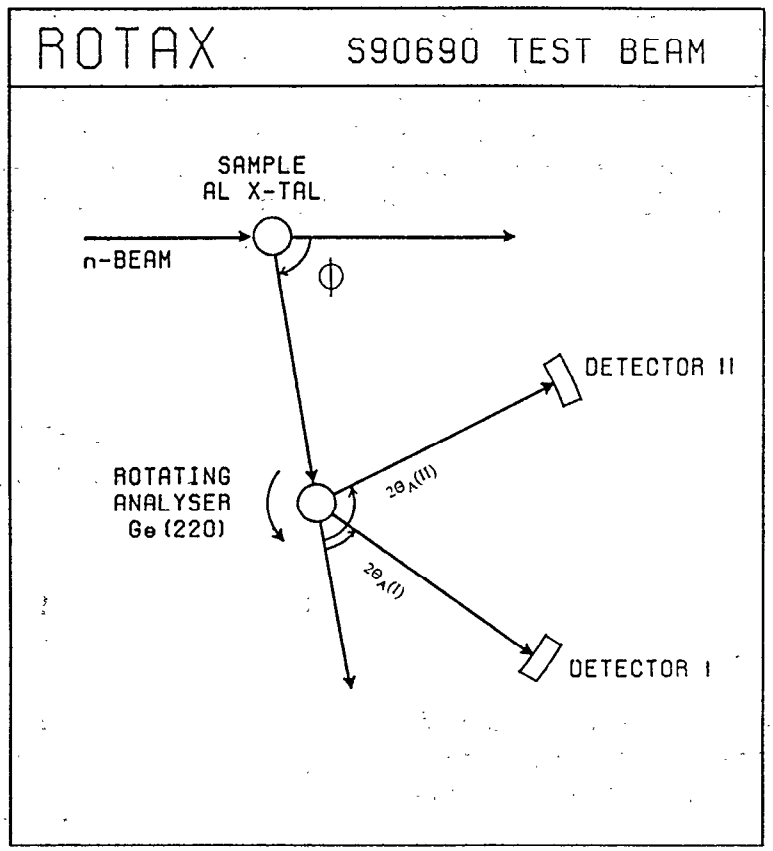


Fig. 2: geometric set-up of ROTAX test assembly.

## III. Calibration, Alignment and Background

Mechanical uncertainties and misaligments in the spectrometer flight paths and especially in the angular setting of the scattering angle $\phi$ and detector angle $2\Theta_A$ with mechanical protractors, had to be determined and gauged. The in-pile neutron flight path was determined by resonance absorption technique, where an auxiliary detector was put to the sample position to measure the incident time-of-flight of the 4.280 eV and 10.360 eV neutron energies being absorbed by a lead foil, placed directly in the white incident beam. The secondary flight paths could be measured directly with sufficient accuracy. Hence, the effective scattering angle $\phi$ as well as the detector angle $2\Theta_A$, were obtained straight foreward from neutron Bragg diffraction:

$$2\,d\,\sin\theta = \lambda = \sqrt{K_0 / E} = \sqrt{2\,K_0 / m_n}\;\; t_0 / L_0 \qquad (1)$$

with $K_0 = h^2/2m_n = 81.8054$ Å$^2$·meV, $L_0$ and $t_0$ the total flight path and total time, $m_n = 10.4541$ meV·msec$^2$·m$^{-2}$ the neutron mass and E, $\lambda$ the neutron energy and wavelength. d is the lattice spacing of the Bragg plane under consideration and $\theta$ the half of the Bragg scattering angle. Thus, $\phi$ is gauged by Bragg diffraction from the Al-sample ($\theta = \phi/2$), whereas the detector angle $2\Theta_A$ is gauged by placing the Ge-analyser on top of the ROTAX motor into the direct neutron beam ($\theta = 2\Theta_A/2$). This diffraction mode of ROTAX was also used to lign-up the Al-sample and Ge-analyser crystal and to determine the offset values and zero setting of the $\phi$- and $2\Theta_A$- circles, respectively (cf. fig. 3).

The Bragg pattern of a Ni-powder sample has been used to calibrate and normalise the efficiency of the different $^3$He-gas tube counters. Some rather poor shielding of approx. 2 mm $B_4C$ and 0.3 mm Cd sheets has been used to protect the detectors against strange irradiation from the air scattering of the primary beam and against the albedo of surrounding material, namely the steel ground plate, which was illuminated by the sample's Bragg star under some obscured scattering angles. Still, there was a lot of fairly isotropic background intensity in the serious spectra.

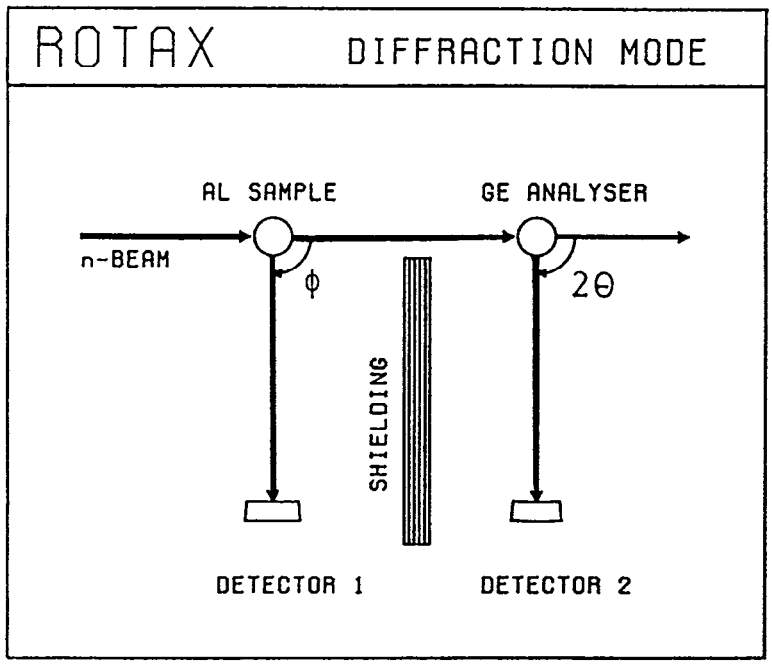


Fig. 3: set-up of ROTAX diffraction mode for spectrometer calibration and aligment.

## IV. Mode of Operation

The flexibility of ROTAX is to almost arbitrarily choose the type of time-of-flight scan in $(Q,\omega)$-space. In our previous papers [1,6,7,9,10] two particular ROTAX-scans, namely the const.-energy and the const.-$\psi$ scan, where the direction of momentum transfer $\vec{Q}/Q$ is fixed, have been discussed in detail. Regarding the corresponding motor performance and motor dynamics, the const.-energy mode of operation is, in general, much more power consuming and more difficult to perform reliably than, for instance, the const.-$\psi$ scan mode. Therefore and in a first step, the const.-$\psi$ mode has been applied for all inelastic scans performed in the test experiments considered here. This is, however, by no means the end of phantasy; in fact, many other scan modes are, in principle, conceivable. For comparison with the corresponding PRISMA-mode of operation measurements with an oriented, but non-spinning idle analyser have also been done parallel to all of the basic "lighthouse modes".

The const.-$\psi$ mode is most adapted to measure excitations in longitudinal polarisation, where the reduced wave-vector $\vec{q}$ is parallel to the momentum transfer $\vec{Q}$. The time-of-flight parabola of energy vs. momentum transfer intersects naturally the extended dispersion scheme of an excitation, e.g. a phonon (cf. fig. 4). The excitation spectrum can be obtained from several Brillouin zones simultaneously and the appropriate choice of scan-parameter $\psi$ will uniquely define a desired point $(\omega_0,Q_0)$. Of course, the same point $(\omega_0,Q_0)$ can also be scanned in const.-energy mode, for instance, but then there is only one intersection of the dispersion curve with the TOF-frames. This situation may change for transverse polarisation (fig. 5), where the constant.-energy scan mode may be advantageous from that point of view.

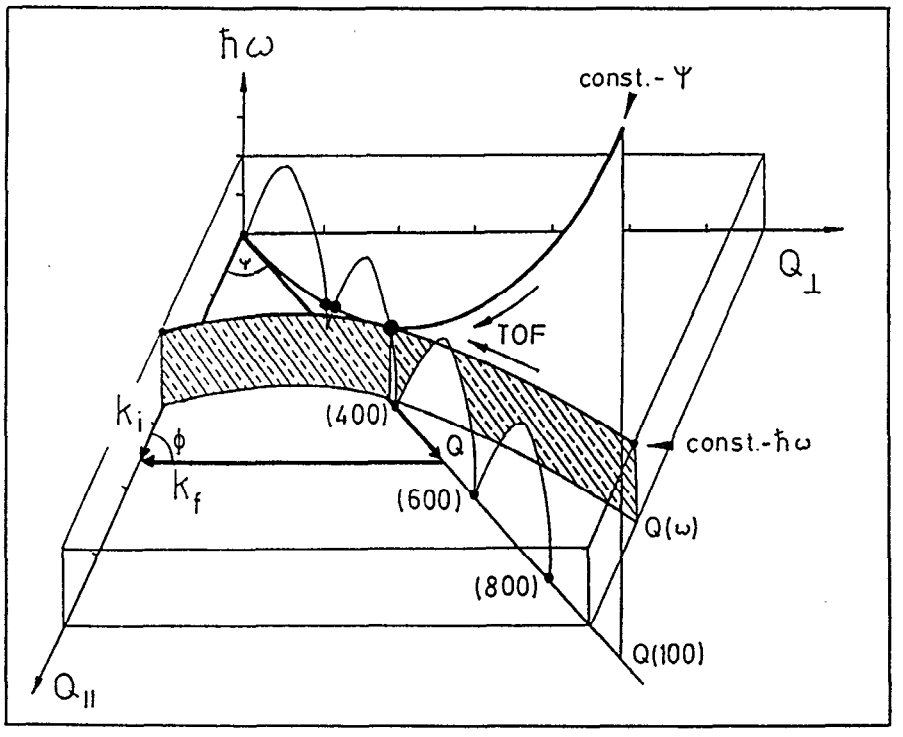


Fig. 4: Time-of-flight curves in $(Q,\omega)$-space for a const.-$\psi$ and const.-$\hbar\omega$ scan. The dots indicate the intersection of const.-$\psi$ parabola with an assumed longitudinal acoustic phonon dispersion as discussed in text.

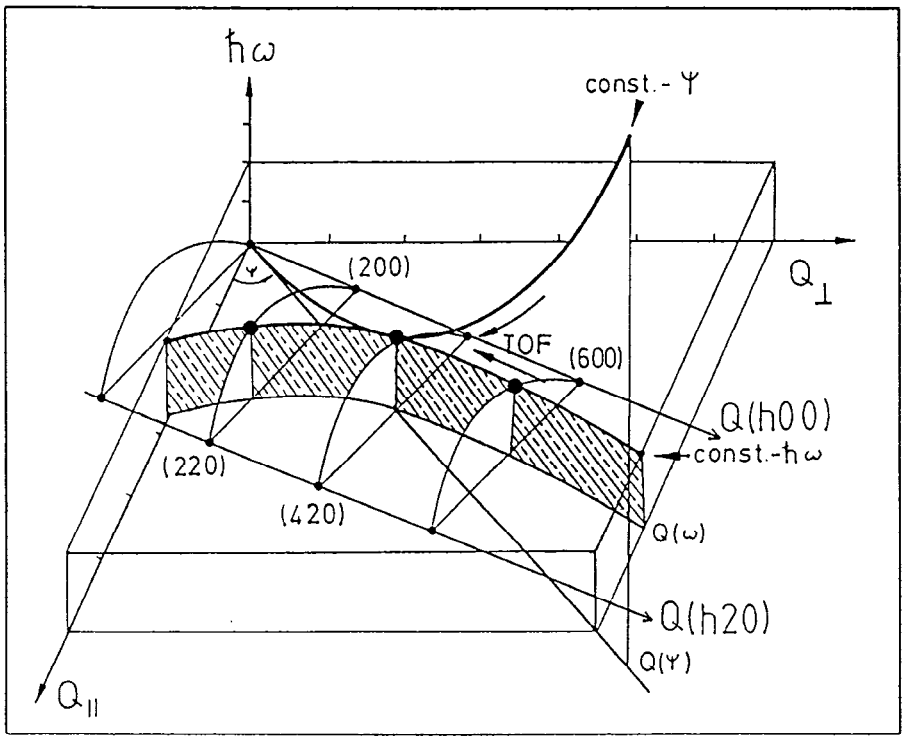


Fig. 5: Time-of-flight curves in (Q,ω)-space for a const.-$\psi$ and const.-$\hbar\omega$ scan. The dots indicate the intersection of const.-$\hbar\omega$ hyperbolic with an assumed transverse acoustic phonon dispersion as discussed in text.

## V. Elastic scattering

Elastic scattering from the Al-Bragg peaks of the <100>-zone has been performed at a scattering angle of $\phi$ = 76.6°. All Bragg reflections of the same crystallographic zone will occur at the same angle $\phi$, however, their Bragg energies are different. Hence, these Bragg peaks are to be observed at different time channels of total neutron time-of-flight. On conventional TOF-X spectrometers with one idle analyser, only one of these Bragg peaks can be observed in due course, if the analyser angle is set properly to this Bragg energy. For comparison purposes we have done this with our test assembly as well, using the Ge-(400) reflection at $2\Theta_A = 52.6°$ to display the Al-(400) Bragg peak on the detector (fig. 6). We may call this mode the "PRISMA mode" of ROTAX, because this is exactly what PRISMA at ISIS or MAX at KENS would do on each single one of their plenty analyser arms. We have had one arm only, equipped with one analyser crystal on the S9 test assembly, however, the ROTAX principle enforced us to do more with it: By setting both arms of the two detector arrays to angles of $2\Theta_A(I) = 33.6°$ and $2\Theta_A(II) = 52.6°$ the Al-(600) and Al-(400) Bragg reflections could be observed simultaneously (fig. 7). In fig. 7 the intensities obtained from both detectors arms has been added to one file, just to clarify and simplify the presentation of the figure. ROTAX, i.e. the Ge-analyser crystal, has been spinned for elastic scattering in order to catch the two Al-Bragg energies of 117 meV and 52 meV, respectively. Both, the Ge-(400) and the Ge-(220) reflections have been used and of course, this does only affect the motor performance and dynamics, not the obtained neutron scattering intensity at the detector.

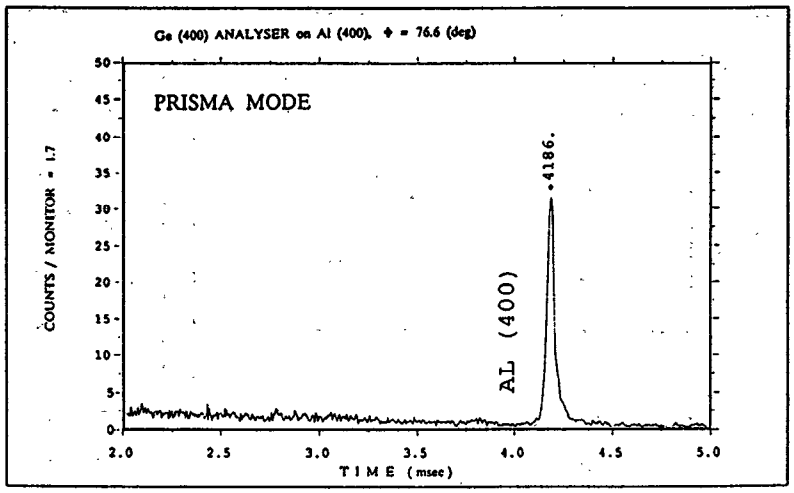


Fig. 6: Al-(400) Bragg peak as observed with Ge-(400) analyser plane in PRISMA mode at $\phi = 76.6°$ scattering angle.

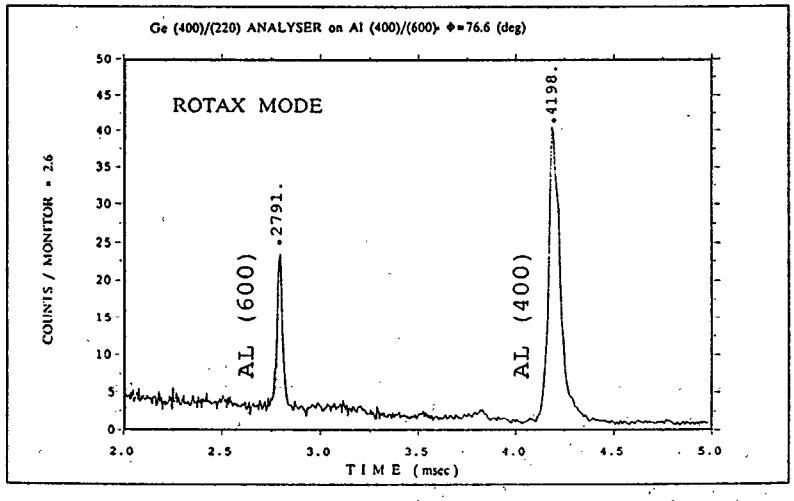


Fig. 7: Al-(400) and Al-(600) Bragg peaks as observed either with Ge-(400) or Ge-(220) analyser plane in ROTAX elastic lighthouse mode at $\phi = 76.6°$ scattering angle.

In case of elastic scattering, there is no difference between const.-energy and const.-$\psi$ scans with respect to the motor performance. However, the motor dynamics depends significantly on the appropriate choice of analyser reflection plane. The particular scan discussed here, performed much better when using the Ge-(220) reflection as analyser, because of its lattice spacing of $d_A = 1.999$ Å, where the average rotation frequency of the analyser is much more adapted to the ISIS pulse repetition frequency. Hence, the mean square acceleration of the analyser is less when using Ge-(220) instead of Ge-(400) reflection. Fig. 8 illustrates these two cases of motor dynamics and performance. The required and the actually achieved values for $\Theta_A(t_A)$ at the time $t_A$, when neutrons arrive at the analyser, and its derivatives $d\Theta_A/dt_A$, $d^2\Theta_A/dt_A^2$ are plotted, the dashed lines mark the desired time channels for the Al-Bragg energies of 117 and 52 meV, respectively. There is no general rule to determine the optimum analyser reflection. It rather depends on the experimental condition and required parameters, such as sample scattering angle $\phi$, neutron energies to be scanned, actual motor performance and reliability under the terms of strict synchronisation with the neutron source, intensity considerations etc. Therefore, it is essential also to look at the actual angular decoder values of the analyser's motor and to permanently monitor these values in the data aquisition system of ROTAX.

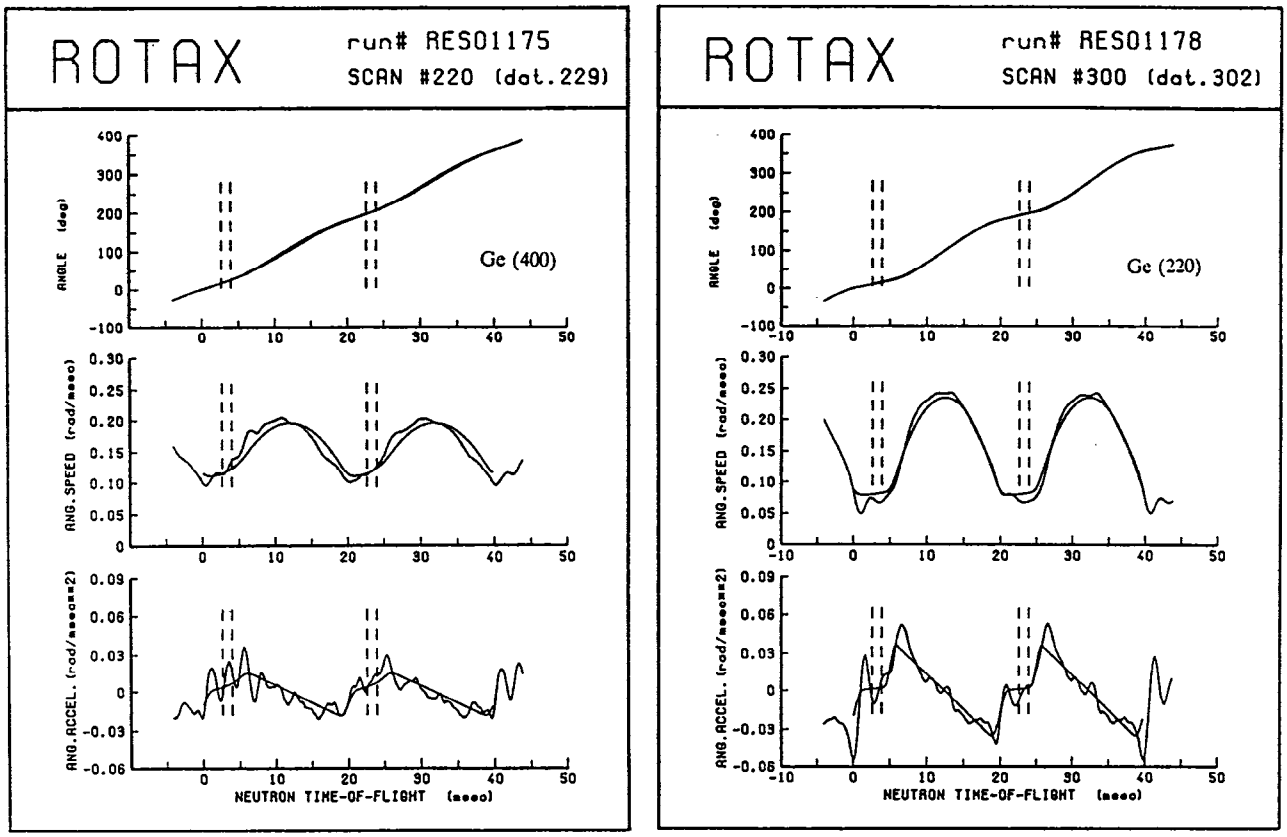


Fig. 8: ROTAX motor performance to the Al-(400)/(600) Bragg scans of fig. 7, a) with Ge-(400) and b) with Ge-(220) analysing plane. The analyser angle $\Theta_A$ and its derivatives is plotted for 1 motor revolution in the time of 2 ISIS cycles. The dashed lines indicate the time channels of interest for the (400) and (600) Bragg energies of aluminium.

When using the Ge-(220) plane, the range of $2\Theta_A$ is naturally smaller than for the Ge-(400) plane. In fact, it was possible to cover the range of $2\Theta_A$ between 15° and 60° with the JULIOS szintillator bank and to catch three Al-Bragg lines, namely the Al-(400), (600) and (800) reflection, simultaneously, i.e. within one shot.

## VI. Inelastic Scattering

ROTAX is primarily dedicated to inelastic scattering, thus it is essential to demonstrate its capability in this field as well. The longitudinal acoustic phonons LA[100] of aluminium have been measured by means of const.-$\psi$ scans in energy loss for the neutrons, i.e. $k_f<k_i$. Fig. 9 illustrates the experimental condition: in the upper part of the figure the alimunium LA[100] dispersion [11] is plotted together with the const.-$\psi$ TOF-parabolas for various values of the parameter $\psi$. The effective position of the two detector arrays is indicated. In the lower section of fig. 9 the Q-space with the Brillouin zone of the actual Al-lattice is shown together with the scattering triangle for the elastic and inelastic condition.

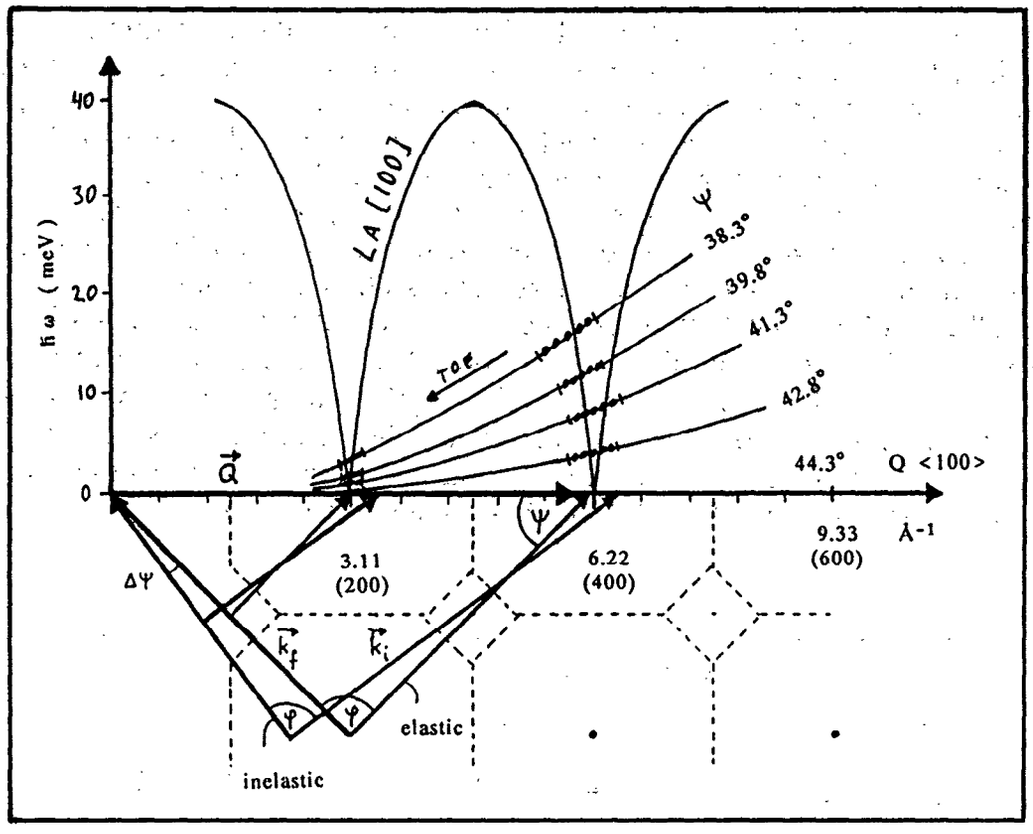


Fig. 9: LA[100] phonon dispersion of aluminium, Q-space and ROTAX const.-$\psi$ parabolas of the test experiment discussed in text.

For const.-$\psi$ scans the obtained energy transfer $\hbar\omega$ in terms of scattering angle $\phi$ and scan parameter $\psi$ is given by [1]:

$$\hbar\omega = \frac{\hbar^2 Q^2}{2 m_n} \frac{\sin(2\psi + \phi)}{\sin\psi} = \frac{\hbar^2 Q^2}{2 m_n} (\cos 2\psi + \mathrm{ctg}\,\phi \sin 2\psi) \qquad (2)$$

Thus, we obtain:

$$2\psi + \phi \begin{cases} < 180° & \text{inelastic scattering, energy loss of the neutrons} \\ = 180° & \text{elastic scattering} \\ > 180° & \text{inelastic scattering, energy gain of the neutrons} \end{cases}$$

At a scattering angle $\phi = 91.4°$ LA[100] phonons of aluminium have been observed in the (200) and (400) Brillouin zones at const.-$\psi$ varying between $\psi = 44.3°$ and $\psi = 38.3°$ in step of $\Delta\psi = 1.5°$. A typical result is shown in fig. 10, where we present a multi-plot of the unfiltered original raw-data without any background correction or monitor normalisation, just as obtained directly from each of the nine detector spectra (in fact, counter #1 was idle). Counter #2-#5 were grouped in detector array II at an angular position of $2\Theta_A(II)=99.4°$, whereas the others were grouped in detector array I at $2\Theta_A(I)=44.5°$ (cf. fig. 2). Apparently, there is the isotropic elastic incoherent scattering at time channels of 9.8 msec and 4.9 msec total time-of-flight due to the Al-(200) and Al-(400) lines, respectively. This isotropic

incoherent elastic line originates from the fluorescense of the germanium crystal when it is irradiated by the very intense Bragg peaks of the aluminium sample. From either these elastic lines phonon scattering intensity is seen to emerge very clearly in both detector arrays. In fact, the phonon at 4.8 msec measured in the (400)-Brillouin zone is characterised by $\hbar\omega$ = 4 meV energy transfer and $\vec{q}$ = 0.04 reduced wavevector, the other one at 9.2 msec, measured in the (200)-Brillouin zone, is found at $\hbar\omega$ = 1 meV and $\vec{q}$ = 0.01. All other peaks, bumps and hubbles of intensity shown in the spectra in fig. 10 are due to background scattering, because of weak shielding and the albedo of the steel ground-plate mentioned above. Real inelastic scattering on ROTAX has, in fact, to fulfill a 4-fold coincidence, because the incident and final neutron energy as well as the detector position and appropriate analyser Bragg angle at the desired time $t_A$ of neutron arrival at the analyser must all fit together according to the scattering laws of energy and momentum conservation. In general, background scattering does not fulfill all these requirements at once.

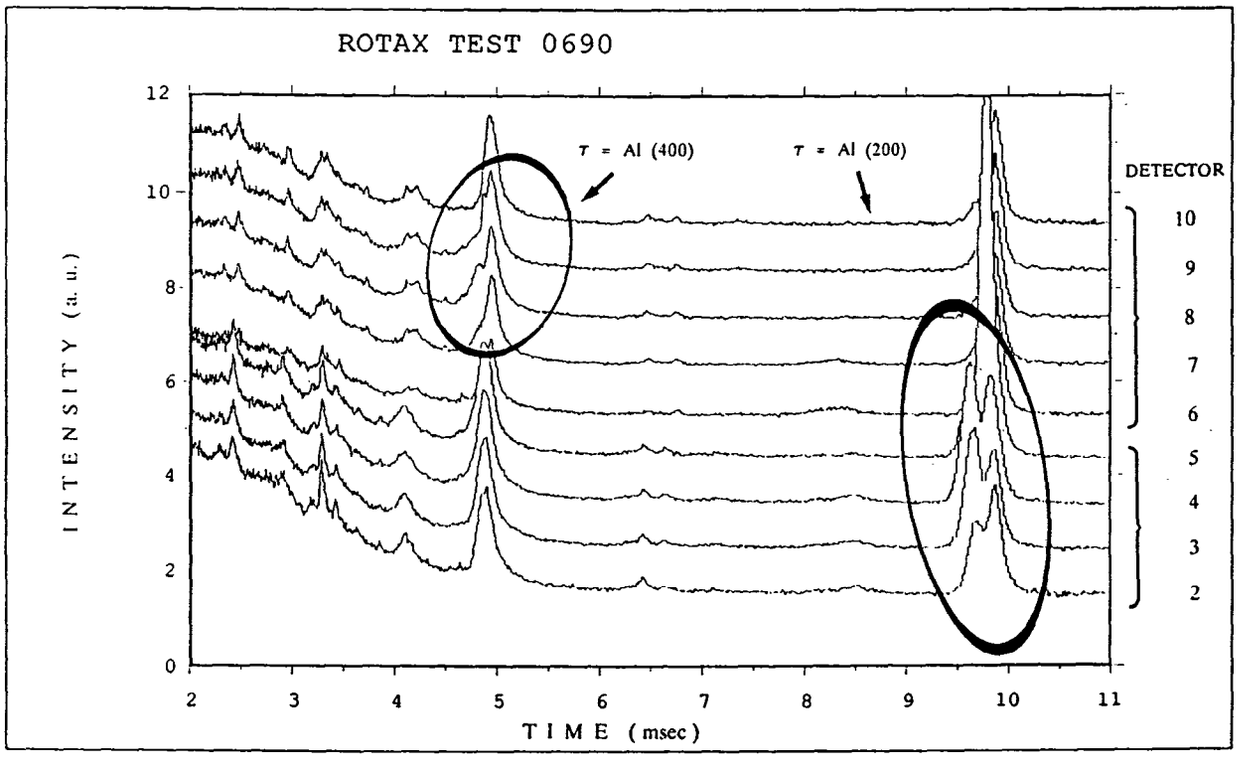


Fig. 10: Raw-data TOF-spectra of two Al-phonon lines of a const.-$\psi$=42.8° scan with Ge-(220) at $\phi$=91.4° scattering angle.

Although in energy loss of the neutrons, inelastic scattering occurs prior to elastic scattering, because of two reasons: a) the analyser is spinning with increasing $\Theta_A$, hence decreasing analysing final energy, b) inelastic scattering occurs from accordingly more energetic and thus faster incident neutrons. A more distinct presentation of the experimentally observed phonon lines is given in figs. 11 and 12: fig. 11 shows a window of the original TOF-spectrum for the 4 meV phonon together with an according

background spectrum as obtained from a $2\Theta_A$-offset scan. Fig. 12 presents the 1 meV phonon more pronounced and in addition to the incoherent elastic line plotted in a scale of energy transfer. The elastic line immediately disappears, if the Al-crystal is rocked to another position in $\psi$, where the Bragg beam of divergence $\alpha_1$ does no longer hit the analyser crystal. In fact, this condition is fulfilled and consequently no such incoherent scattering has been found for higher energy transfers or reduced values $\psi<42°$, where $\psi<\psi_{el}-\alpha_1/2$ for $\psi_{el}=(180°-\phi)/2$ (cf. eq. 2 and fig. 13).

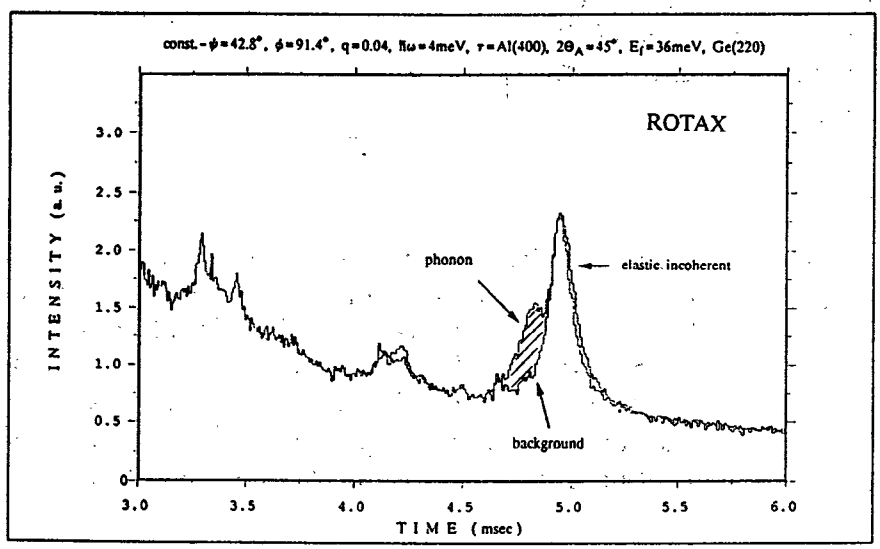


Fig. 11: The $\tau=(400)$, $q=0.04$, $\hbar\omega=4$meV LA[100] phonon of fig. 10 together with a $2\Theta_A$-offset background scan.

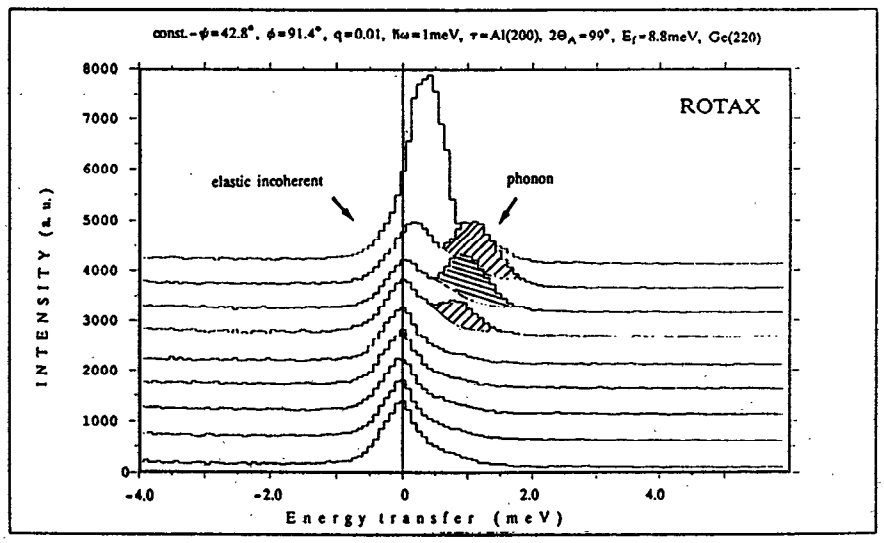


Fig. 12: The Al-(200) incoherent elastic scattering and the $q=0.01$, $\hbar\omega=1$meV phonon of fig. 10.

It is not possible to obtain all these longidutinal phonon modes in the "PRISMA mode" directly. Therefore no PRISMA-type scan of the measurements discussed above can be given for purposes of comparison. This, however, may be regarded as an illustrative example of the advanced scan flexibility on ROTAX!

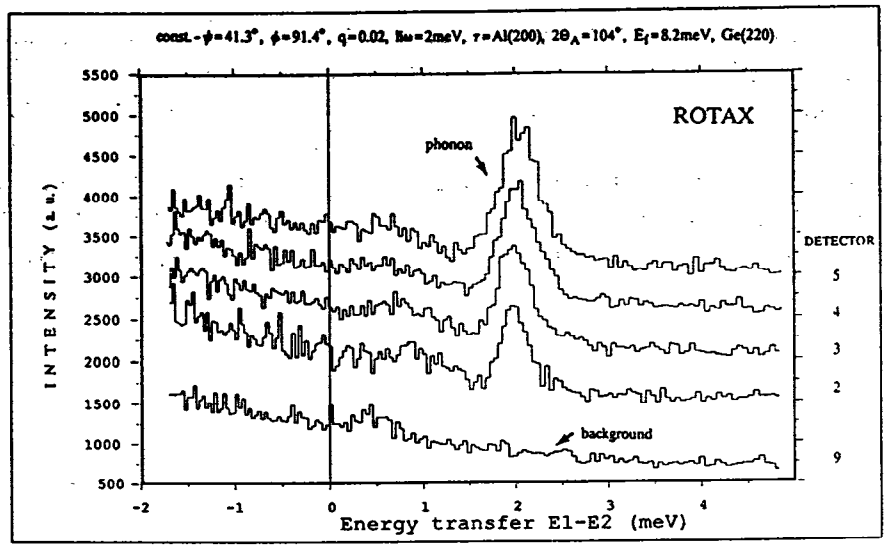


Fig. 13: The $\tau=(200)$, $q=0.02$, $\hbar\omega=2$meV phonon of aluminium without an accompanying elastic incoherent line; scanned with const.-$\psi$ = 41.3° at $\phi$ = 91.4° scattering angle. The Ge-(220) analyser plane was used.

Anyhow, to give an idea about the competition of a ROTAXed "lighthouse mode" versus the "PRISMA mode" of operation, we shall give in the following an example of a tranverse TA[100] phonon scan (cf. fig. 5) of aluminium, taken at $\tau=(410)$ for wavevector $\vec{q}=0.5$[010] and $\hbar\omega=25.4$ meV. In figs. 14 and 15 the inelastic scattering intensity of this zone boundary phonon is plotted vs. energy transfer as obtained from the PRISMA and ROTAX mode, respectively. The intensity has been normalised to the monitor count- rate and corrected for background scattering in either case.

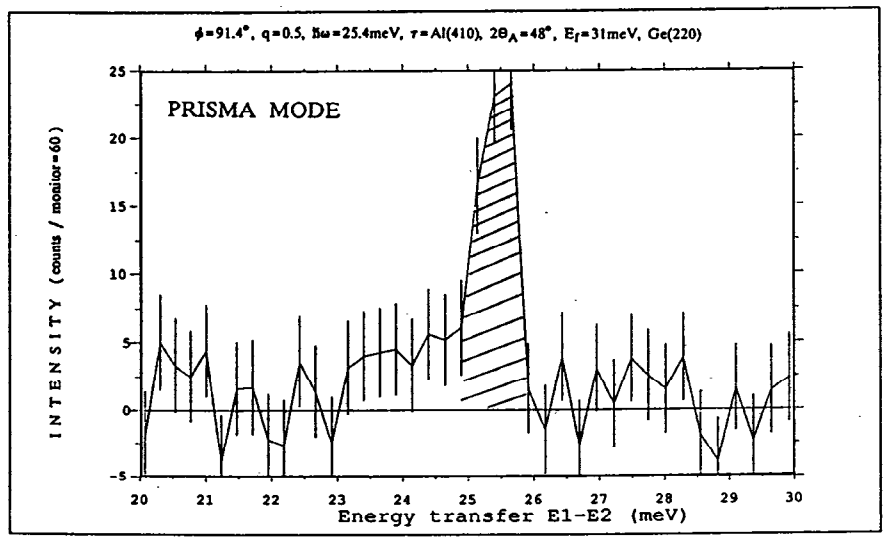


Fig. 14: The TA[100] zone boundary phonon of aluminium at $\hbar\omega$ = 25.4 meV. PRISMA mode at $\phi$ = 91.4° scattering angle with Ge-(220) analyser.

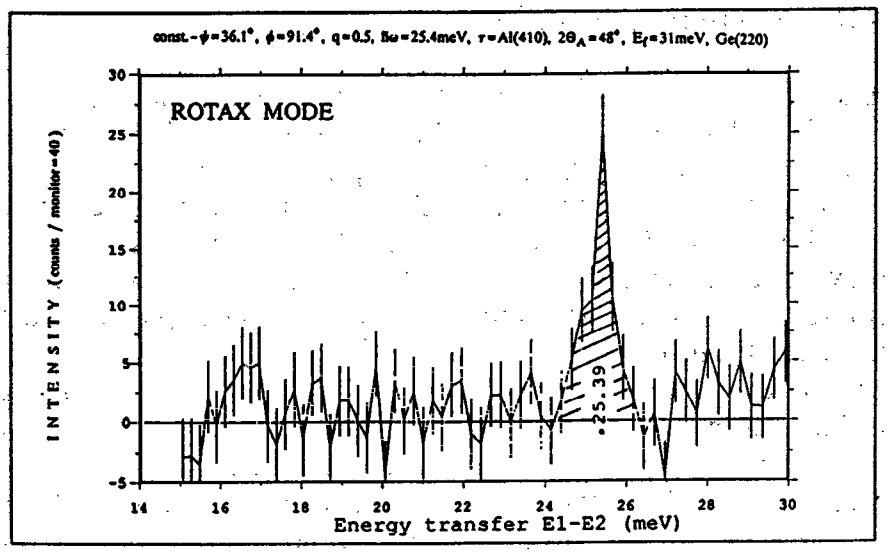


Fig. 15: The TA[100] zone boundary phonon of aluminium at $\hbar\omega$ = 25.4 meV. ROTAX const.-$\psi$=36.1° mode at $\phi$ = 91.4° with Ge-(220)

Apparently, ROTAX performes about equally with PRISMA under the same experimental condition. Further, the actually achieved motor performance should not be omitted for this particular example. The required and achieved values of the analyser Bragg angle $\Theta_A$ and its derivatives are plotted in fig. 16 for one motor revolution in the time of two neutron frames. Of course, the accurate setting of the analyser Bragg angle is of striking importance for the intensity obtained on ROTAX, whereas the accurate performance of the angular speed is of importance for the ROTAX motor regulation government and the angular acceleration is the dominant factor for the torque and power of the motor. The dashed lines in fig. 16 again indicate the desired time channel of best achievable accuracy and, of course, there is only one such time channel of interest for this particular scan, because there is only one excitation line in every neutron frame to be measured.

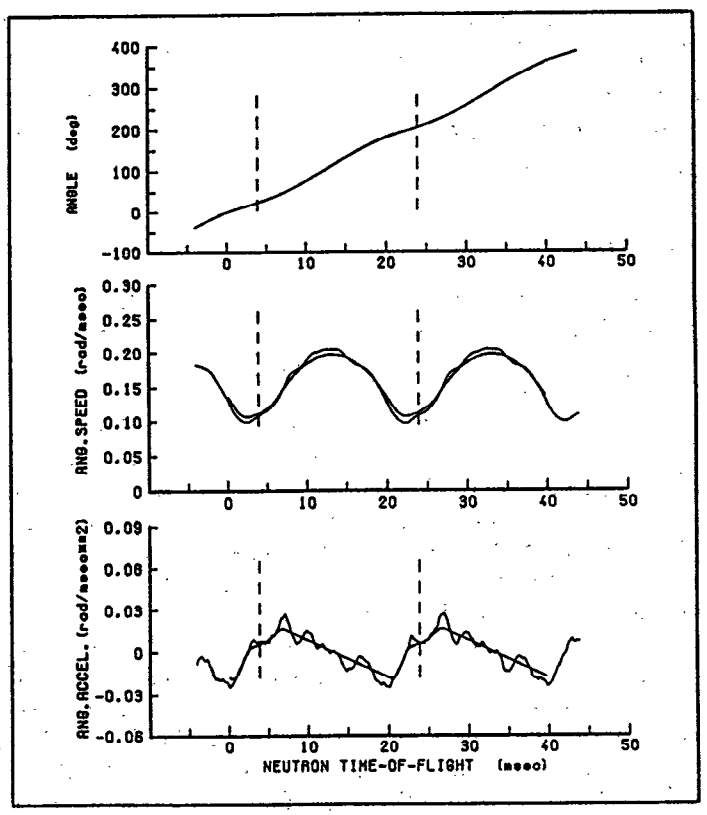


Fig. 16: ROTAX motor performance to the transverse phonon scan of fig. 15. The analyser angle $\Theta_A$ and its derivatives is plotted for one motor revolution in the time of 2 ISIS cycles. The dashed line indicates the time channel of interest.

## VII. Concluding remarks

After more than four years of research, design and development of the fundamental technical devices for ROTAX, i.e. the control unit for its spinning analyser drive, we were able to demonstrate the principle proof on the basic capability and performance of the instrument under realistic neutron scattering conditions. In a two-phase test experiment on the S9 test beam facility at ISIS this success has been achieved with a provisional assembly of the ROTAX spectrometer and with a prototype of the motor control unit. Only minimum effort has been put to background suppression, full detector furnishment, software comfort and experimental elegance, and still phonons have been measured successfully with sufficient intensity and peak-to-background ratio within reasonable counting times. Although the technical development of ROTAX is by no means complete and finished yet, further improvements already being under construction will enhance the reliability and accuracy of the ROTAX drive considerably, we are now in the position to say without any doubt: ROTAX is working and it will fulfill its promisses! We shall now enter the "concrete phase", starting the design and installation of the spectrometer and its bulky components at its finally desired position behind the anglo-italian PRISMA spectrometer on the N2 beam line at ISIS. We expect to become operational in early 1993.


## Acknowledgment

We want to thank all those who have contributed to the success reported above; namely Mr. A J Chappell, Mr. A F Gilleard, Mr. E M Mott and Mr. S M Spurdle (RAL) for their help in the preparation period and their support during the test experiments on S9 at the Rutherford Appleton Laboratory. We also want to thank the ISIS computing group and further, Dr. C J Carlile (RAL) and Dr. C Petrillo (CNR Frascati, Italy) for providing the excellent Al-sample and Ge-analyser crystals. We acknowledge Mr. E Jansen and Mr. R Skowronek (KFA Jülich) for their assistance with the JULIOS szintillator bank, which has been borowed from the Institute of Mineralogy of the Univ. of Bonn, F.R.G. - This work has been performed under the terms of the "Rutherford-Würzburg" collaboration agreement and it has been funded by the German Federal Minister for Research and Technology (BMFT) under contract number 03-Ge2-Wue.


## References


[1] Geick R and Tietze H, Nucl. Inst and Meth. A **249**, 325 (1986)
[2] Robinson R, Eckert J and Pynn R, Nucl. Inst. and Meth. A **241**, 312 (1985)
[3] Tajima K, Ishikawa Y, Kanai K, Windsor C G and Tomiyoshi S, Nucl. Inst. and Meth **201**, 491 (1982)
[4] Andreani C, Carlile C J, Cilloco F, Petrillo C, Sacchetti F, Stirling G C and Windsor C G, Nucl. Inst and Meth. A **254**, 333 (1987)
[5] Steigenberger U, Hagen M, Caciuffo R and Sacchetti F 1990 RAL-90-004 and Nucl. Inst. and Meth. to be published 1990
[6] Tietze H and Geick R, Proc. ICANS IX 1986 CH-Villigen, SIN-rep 3-907998-01-4, 389 (1987)
[7] Tietze H, Schmidt W, Geick R, Samulowitz H and Steigenberger U, Proc. WONSDA II, to be published in IOP Conf. Series 1990
[8] Jansen E, Schäfer W, Szepesvary A, Will G and Kurz R, Physica B **156**, 584 (1989) and references therein
[9] Schmidt W, Tietze H and Geick R, Physica B **156**, 554 (1989)
[10] Tietze H, Schmidt W and Geick R, Physica B **156**, 550 (1989)
[11] Stedman R and Nilson G, Phys Rev. **145**, 492 (1966)

Q(I.M.Thorson): What angular tolerance are you achieving at present?
A(H.Tietze): The present 0.5°, although 0.1° is required and we see how to achieve this.